Pure Appl. Chem., Vol. 81, No. 10, pp. 1783–1798, 2009.
doi:10.1351/PAC-CON-08-09-10
© 2009 IUPAC, Publication date (Web): 17 September 2009

Microphase-separated multicontinuous phase in low-molecular-mass thermotropic liquid crystals*

Kazuya Saito

Department of Chemistry, Graduate School of Pure and Applied Sciences, University of Tsukuba, Tsukuba, Ibaraki 305-8571, Japan

Abstract: Extensive application of chemical thermodynamics to exotic aggregation formed in thermotropic liquid crystals is briefly described. Through thermodynamic analyses and considerations of experimental results on liquid crystals, the unexpected sharing of common properties by thermo- and lyotropic liquid crystals is demonstrated. In some thermotropic liquid crystals, the terminal alkyl chain attached to the molecular core is highly disordered, as indicated by the magnitude of configurational entropy. The molten chain serves as intramolecular solvent (self-solvent), as evidenced by the close similarity between phase diagrams against chain length and composition in the binary system with *n*-alkane. These facts lead to the quasi-binary picture of thermotropic liquid crystals. Consideration of the thermodynamic potential expanded in terms of density fluctuation gives a new insight into the multicontinuous phases formed in simple systems consisting of anisotropic, rodlike particles.

Keywords: entropy; liquid crystals; self-organization; multicontinuous; thermodynamics.

INTRODUCTION

Exotic aggregation structures characterized by the term "multicontinuous" often appear in soft matter such as lyotropic liquid crystals and polymers as a result of microphase separation. Similar structures have also been identified in thermotropic liquid crystals. This paper describes the properties and structures (at the molecular level) of such thermotropic liquid crystals, while putting special emphasis on the roles played by thermodynamic interpretation of both experimental and theoretical aspects.

LIQUID CRYSTAL AND COMPOUNDS OF INTEREST

The term "liquid crystal" means in a broad sense a kind of liquids possessing structure [1]. Usually, the structure induces the anisotropy that is the basis for wide applications of liquid crystals such as display. Liquid crystals are often classified into two groups: thermotropic and lyotropic. The basic mechanisms for achieving liquid-crystalline order are generally assumed to differ significantly between the two groups. That is, the excluded volume effect is crucial in the former while microphase separation dominates in the latter.

Thermotropic liquid crystals appear upon temperature variation. The formation of this type of liquid crystal comes from the strong shape anisotropy of constituent molecules. Indeed, the formation of thermotropic liquid crystals is understood within the unified view of melting of molecular crystals [2–4] as shown in Fig. 1. In the ordered state, molecules are located regularly on a lattice and align their ori-

*Paper based on a presentation at the 20th International Conference on Chemical Thermodynamics (ICCT 20), 3–8 August 2008, Warsaw, Poland. Other presentations are published in this issue, pp. 1719–1959.

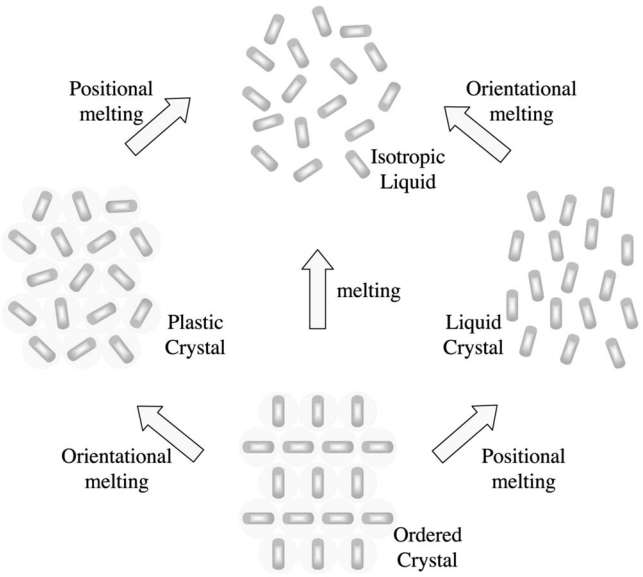

Fig. 1 Melting of molecular crystals (schematic). Depending on the shape anisotropy, the ordered crystal melts via liquid-crystalline state (positionally melted but orientationally ordered state), plastic crystalline state (orientationally melted but positionally ordered state), or directly to the isotropic liquid.

entation. Many compounds like benzene undergo a melting transition in a single step. However, if the shape of the molecule is highly anisotropic, the melting (disordering) of the position can take place at a lower temperature than that of the orientational melting. The resultant liquid is anisotropic liquid, i.e., a liquid crystal. Thus, usually molecules forming thermotropic liquid crystals are like a rod or disc. Indeed, the appearance of liquid crystal was theoretically shown first by Onsager in 1949 for aggregates of rigid-rods [5]. This type of liquid crystal is the simplest liquid crystal called "nematic" (abbreviated as N). Upon heating the liquid crystal further, the orientation also melts, resulting in normal, isotropic liquid. Although there are a variety of liquid-crystalline phases [1], their classification and description are beyond the scope of the present paper. It is sufficient at this stage to note that smectic (Sm) phases have layered structure with fluidicity inside layers. In contrast to the formation of liquid-crystalline states, an orientationally melted but positionally ordered state can appear upon the way of melting. This state is called "plastic crystal". The most famous compound showing a plastic crystalline state is, nowadays, buckminsterfullerene (C_{60}) at room temperature.

Lyotropic liquid crystal, on the other hand, appears upon changing concentration [1,6,7]. Accordingly, the lyotropic liquid crystal has at least two components. Usually, amphiphilic molecules or surfactants are involved in the formation of lyotropic liquid crystals. A typical example of lyotropic liquid crystal is a concentrated soap solution. Due to the so-called microphase separation, a variety of structures are formed in the solution depending on concentration. Hexagonal and lamellar phases are representative of lyotropic liquid crystal. Rod-shaped micelles align in a close-packed way in two dimensions, resulting in hexagonal symmetry in the former while flat bilayers of surfactants stack in one dimension in the latter.

Compounds treated in this paper are 4'-*n*-alkoxy-3'-nitrobiphenyl-4-carboxylic acid [abbreviated as ANBC(*n*) hereafter, with *n* in parentheses being the number of carbon atoms in the alkyl chain if necessary] [8] and 1,2-bis(4'-*n*-alkoxybenzoyl)hydrazine [BABH(*n*)] [9] shown in Fig. 2. Both molecules consist of a relatively rigid core part and long alkyl chain(s). ANBC molecules dimerize in (normal crystalline and) liquid-crystalline states to form a doubled structure like BABH [10]. Consequently, the particle forming liquid-crystalline phases consists of a hard rodlike core and long chains at both ends.

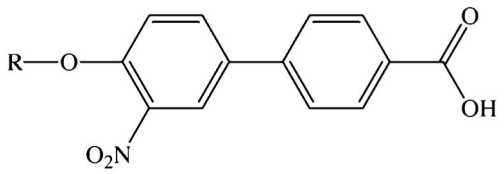

ANBC(n) (R = C_nH_{2n+1})

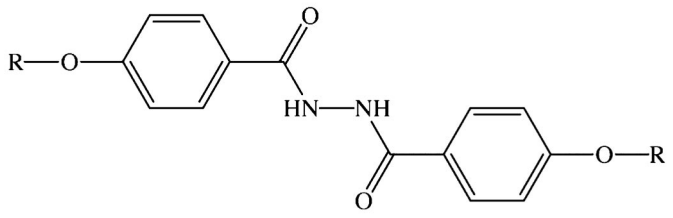

BABH(n) (R = C_nH_{2n+1})

Fig. 2 Molecular structures of cubic mesogens, ANBC(n) and BABH(n). The molecules of ANBC(n) are dimerized in crystalline and liquid-crystalline states through hydrogen bonds between carboxylic acid parts, resulting in a centrosymmetric structure similar to that of the BABH(n) molecule.

Besides, a strong interaction in the lateral direction is expected for both, that is, the dipole–dipole interaction in ANBC and hydrogen bond in BABH. Doubled structure and strong lateral interaction are widely observed in mesogens that form similar multicontinuous structures to those discussed in the following [11].

The phase diagrams of ANBC [12] and BABH [13] are shown against the alkyl chain length in Fig. 3. Two regions indicated as *Ia3d* (No. 230) and *Im3m* (No. 229) correspond to cubic phases having multicontinuous structures. As is evident from the numbers for the space groups, the multicontinuous structures have quite high symmetries. It is noteworthy that some members such as ANBC(26) [14] show a phase transition between two cubic phases with different symmetries on temperature variation.

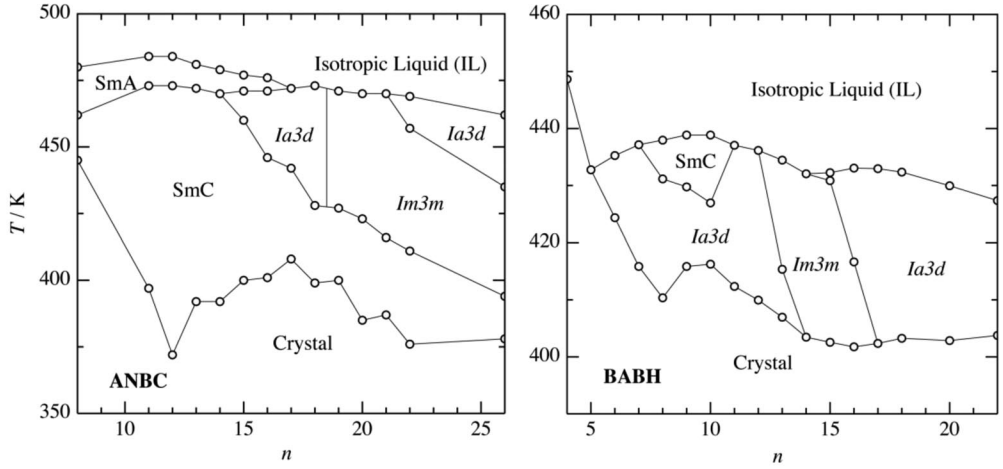

Fig. 3 Phase diagram of ANBC (left) [12] and BABH (right) [13] as a function of alkyl chain length (n). SmC, smectic C phase; *Ia3d*, cubic phase with *Ia3d* symmetry (gyroid phase); *Im3m*, cubic phase with *Im3m* symmetry; SmA, smectic A phase; IL, isotropic liquid.

MULTICONTINUOUS STRUCTURES

The basic structure of the *Ia3d* phases is believed to have a close connection with a continuous surface called gyroid shown in Fig. 4a. Gyroid is a single continuous surface with three-dimensional periodicity. It divides the space into two. A jungle gym can be placed in each space as shown in Fig. 4b. These jungle gyms extend over the whole space and are interwoven. This type of structure is called "bicontinuous". Two descriptions using the surface dividing the space into multiple parts and using multiple jungle gyms are complementary to each other. These positions correspond to locations of some parts of molecules when we discuss the molecular aggregation modes, as will be done later.

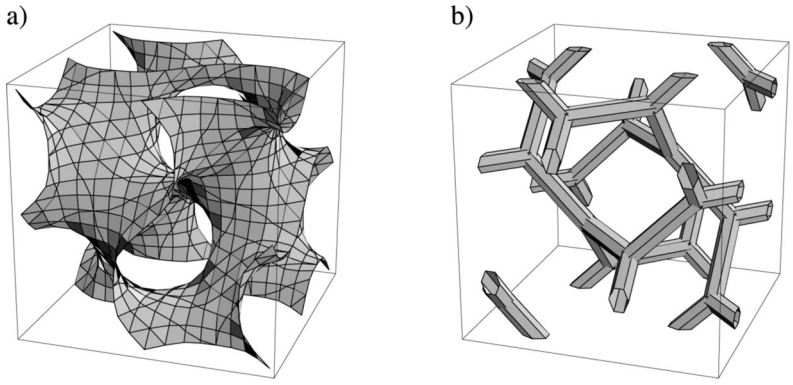

Fig. 4 Two complementary descriptions of the gyroid phase (with *Ia3d* symmetry). (a) gyroid (TPMS); (b) jungle gyms embedded in each side of the gyroid.

Mathematically, the gyroid is characterized as a triply periodic minimal surface (TPMS) [15]. A minimal surface is one with minimum surface area under a given frame. The most familiar example of minimal surfaces is a soap film. In this context, the appearance of the gyroid phase is intuitively acceptable for microphase-separated systems such as lyotropic liquid crystal and block copolymers. Indeed, the bicontinuous phase, most often the gyroid phase, widely appears in such systems [6,7,16]. There are some theories predicting the appearance of bicontinuous phases [17–20]. That is, there is some understanding for the gyroid phase formed in microphase-separated systems. It is noted that, in lyotropic liquid crystal and block copolymers, the phase diagram is essentially symmetric against the composition and the multicontinuous phase appears in the region where the composition is slightly deviated from the equivolume.

The gyroid belongs to a family of TPMS's related by a mathematical transformation (Bonnet transformation), which maintains local geometry at every point on the surface [15]. Consequently, the hypothetical structure characterized by other related TPMSs (P and D surfaces) is expected to have comparable stability if the geometry of the TPMS governs the stability. This offers an interesting issue why the gyroid phase is so common in comparison with infrequent appearance of others. This issue will be discussed later.

It is noted that an Sm phase in thermotropic liquid crystal (and a lamellar phase in lyotropic liquid crystal) can also be described by using flat surfaces. By deforming surfaces and joining them appropriately, we get a gyroid. The essential difference is, therefore, connectivity or topology.

PHYSICAL PROPERTIES OF THE MULTICONTINUOUS PHASE

Heat capacities of some compounds from ANBC and BABH, and related series, were measured by adiabatic calorimetry from liquid helium temperature [21–25]. The results on ANBC(22) [24], which

undergoes a phase transition from the cubic *Im3m* phase to the cubic *Ia3d* phase at 454.13 K, are shown in Fig. 5 as an example. All phase transitions are clearly detected. Although it is hard to recognize from this figure, smooth extrapolations of heat capacities of the SmC phase and the cubic *Im3m* phase clearly show a negative difference at the transition temperature on heating. Namely, the heat capacity of the *Im3m* phase is smaller than that of SmC phase. In many compounds, the heat capacity is larger in the higher-temperature phase than the lower-temperature phase. The negative jump in heat capacity, therefore, implies a somewhat interesting situation. As for the phase transition between two cubic phases, the difference in heat capacity is also negative. In other compounds in the ANBC series, the heat capacity of a cubic phase, irrespective of the symmetry, is smaller than that of the SmC phase located on the low-temperature side [22,23,25]. In lyotropic liquid crystals formed in binary systems between a non-ionic surfactant and water [26,27], the cubic phase shows smaller heat capacity than the neighboring liquid-crystalline phases. This suggests that the cubic phases have smaller heat capacity than liquid-crystalline phases lacking a multicontinuous structure.

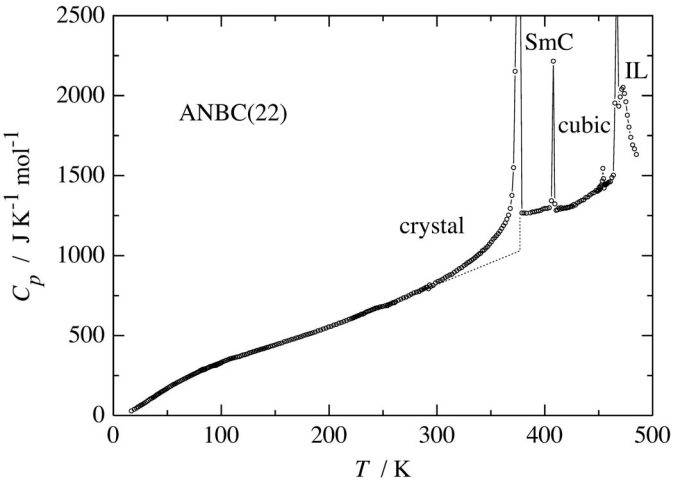

Fig. 5 Experimental molar heat capacities of ANBC(22) measured by adiabatic calorimetry [24]. Dotted line is the normal heat capacity to separate the premelting effect.

As is well known, heat capacity is proportional to fluctuation in enthalpy or entropy [28]. Consequently, the smaller heat capacity indicates the suppressed fluctuation in the cubic phases. The most probable cause for this is the characteristic topology. That is, the cubic phase has a three-dimensionally connected internal structure. This connectivity suppresses the fluctuation. In good agreement with this, the cubic phase is mechanically hard [29–32]. Recently, this topological rheology has been discussed theoretically [33]. It is emphasized that we have no need to know how molecules are packed in a complicated structure such as the gyroid phase for this discussion, by virtue of the phenomenological nature of thermodynamics.

QUASI-BINARY PICTURE OF THERMOTROPICS

In Fig. 5, a clear premelting effect can be recognized [24]. Although the increase in heat capacity in the premelting region is present even in small molecules, the effect in the present case is strong with a large temperature range. This implies that something special happens in this temperature region. By drawing a baseline while considering intramolecular and lattice vibrations, and a small contribution by thermal expansion, we extracted the excess heat capacity due to the premelting effect. By integrating the excess

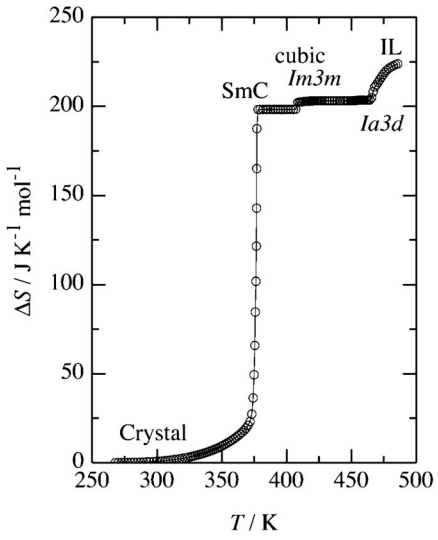

Fig. 6 Excess entropy due to premelting and phase transitions of ANBC(22).

heat capacity against logarithmic temperature, the excess entropy gain is obtained as shown in Fig. 6. The excess entropy shows a large increase upon the transition from the crystalline phase to SmC liquid-crystalline phase and remains at ca. 200 J K^{-1} mol^{-1} in liquid-crystalline states.

To analyze the magnitude of the excess entropy, the "entropy capacity" of alkyl chain is considered [34,35]. As alkyl chains are flexible, they can reserve a large amount of entropy. Indeed, the length dependence of entropy of fusion of *n*-alkanes shows excellent linearity, though separately for odd and even members due to the so-called odd-even effect. From the slope, the entropy capacity is deduced as 10.3 J K^{-1} (mol of methylene)$^{-1}$ [34], which roughly corresponds to *R*ln3. The intercept on the entropy axis corresponds to the contribution of a methyl group. The contribution of the core parts should lie in-between the entropy of fusions of *p*-quinqephenyl (the dimerized case even in the isotropic liquid) and that of biphenyl (monomeric case) [36]. Using these contributions, we can estimate the maximum entropy of fusion as 270 J K^{-1} mol^{-1} for ANBC(22). This is certainly larger than the experimental excess entropy. We must, however, consider that the methylene groups close to the core would not completely melt. Figure 6, therefore, shows that the alkyl chain is already highly disordered in liquid-crystalline states.

What is the role of this disordered chain? To see this, we compared the phase diagrams of neat and binary systems [37]. In comparison, the abscissa was taken as the number of carbon atoms of the alkyl chain in the neat system and the number of paraffinic carbon atoms in the system. The phase diagrams of ANBC(16)-*n*-tetradecane and ANBC(18)-*n*-tetradecane showed close similarity with the neat system in, at least, the overall feature of phase diagram. As *n*-tetradecane is a real solvent, this similarity clearly shows that the intramolecular chain serves as solvent. Later, Kutsumizu et al. [38] performed more detailed studies and confirmed that delicate points are reproduced: induction of a cubic phase in ANBC(14) and change in symmetry of the cubic phase were demonstrated by adding small amount of alkane. These comparisons naturally lead us to a "quasi-binary picture of thermotropics" [39]. That is, at least some of the thermo- and lyotropic liquid crystals share properties and mechanism responsible for the formation of liquid-crystalline order, plausibly. The quasi-binary picture was quantitatively assessed later by Yoneya et al. [40].

It is noted that no induction of a cubic phase was observed in the ANBC(8)-based binary system upon adding a large amount of *n*-tetradecane. This suggests that each part acting as a chain or a core does not simply correspond to the chemical structure [37]. Namely, the effective core necessary for the

formation of cubic phases is larger than the aromatic ring part, containing carboxylic acid groups inside. This is qualitatively consistent with the restricted mobility of the methylene groups in the vicinity of the aromatic ring as discussed above

Δ*S* ANALYSIS AND INVERTED-PHASE SEQUENCE

As noted before, the appearance of the liquid-crystalline state was theoretically shown by Onsager in 1949 for aggregates of rigid-rods [5]. Most succeeding theories also assume the rigid-rods. In contrast, most real mesogenic molecules have long alkyl chains. Then, the question arises what is the role of chains? We already find one answer in the previous section: The chain serves as intramolecular solvent. Here, we see another role played by chains.

According to Boltzmann's principle, entropy has a clear microscopic meaning. In a simple order-disorder transition, for example, the entropy of transition reflects the difference in the disorder intrinsic to the two phases below and above the transition temperature. In the present case, we consider a liquid-crystalline system consisting of molecules. If the molecule behaves as a rigid particle as a whole, the entropy of transition would have a definite magnitude. This is, however, not the case. The ratio of entropies of transition from the SmC phase to SmA phase amounts to 1.7 for ANBC(12) and ANBC(11) [41]. Only one methylene affects drastically the entropy of transition. We know that the ANBC molecules dimerize in liquid-crystalline states [10], and the dimer consists of a rigid core at the center and flexible chains at both ends. The simplest way to understand the large difference in the entropy of transition is that the slope against the chain length is the contribution of the chain as in the case of the fusion of *n*-alkanes [23,24,35,42].

Ideally, the expected chain-length dependence is as follows [35,42]. At the long-chain limit, the entropy of transition linearly depends on the chain length. The slope is the difference in the entropy of chain between the two phases concerned. At the short-chain limit, on the other hand, the entropy will saturate to the magnitude of the contribution of core. We refer to this type of analysis as "Δ*S* analysis". It is noted that the method is applicable in any combination of two phases exhibited by compounds having long alkyl chain(s).

The slope itself in the Δ*S* analysis is the difference in entropy per methylene in two phases. From the viewpoint of molecular dynamics in liquid crystal, this quantity is of great interest because the motional degrees of freedom of the chain are intramolecular in nature and beyond the scope of the rigid-rod model. The present method of analysis is unique with respect to the time scale covered in the study of chain dynamics. Spectroscopies such as NMR are widely used to study molecular dynamics. Each spectroscopic method has a characteristic time scale, by which the molecular dynamics is successfully sensed. The characteristic time scales of spectroscopies are generally equal to the inverse of the frequency used. For NMR, which is widely used and may be the most powerful method, it is 10^{-8}–10^{-10} s. On the other hand, as the calorimetric method is based on thermodynamics, the time scale is extremely long, just as sensed by our daily life. The characteristic time is about 10^3 s. Very slow dynamics, therefore, is favorably studied. Besides, this time scale of thermodynamics implies the lower limit of molecular dynamics that can be detected. Fast dynamics (e.g., that detected by NMR) is also covered by the calorimetric method, though no information is available concerning the time scale of the dynamics.

Now, we apply the Δ*S* analysis to the SmC–cubic phase transitions in ANBC and BABH [23]. The point of interest here is the phase sequence seen in Fig. 3 [12,13]. In ANBC, the cubic phase locates at the high-temperature side of the SmC phase. In contrast, the sequence is reversed in BABH. Figure 7 is the plot of the entropy of transition from the SmC phase to a cubic phase per particle [9,23,24,41]. As the cubic phase locates at the low-temperature side of the SmC phase in BABH, the entropy of transition in this plot is negative.

In ANBC, there is an inflection in the chain-length dependence because there are two different cubic phases (*Ia3d* and *Im3m*) depending on the chain length. The chain-length dependence shows good

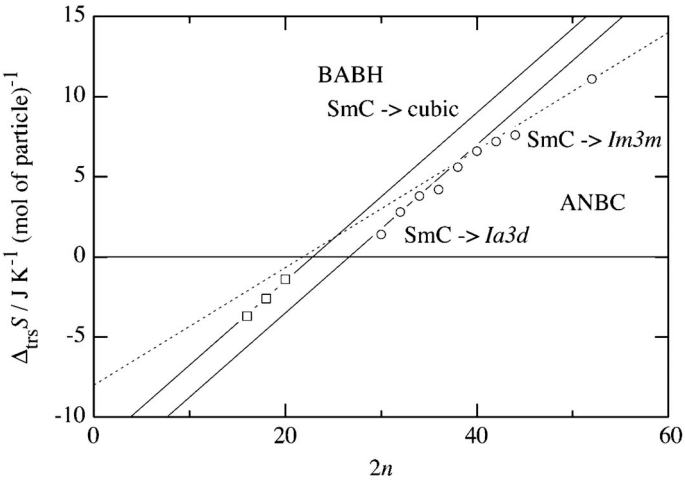

Fig. 7 Entropies of transition per mole of particle (dimer for ANBC and molecule for BABH) from the SmC phase to a cubic phase (*Ia3d* or *Im3m* phase) as a function of 2*n* of ANBC(*n*) and BABH(*n*) [24]. Due to the inverted phase sequence, the entropy of transition is negative in BABH. Solid and dotted lined are guides for eyes.

linearity in all three series with positive slope. This means that the chain is more disordered in cubic phases than in the SmC phase. Similar slopes for SmC–cubic *Ia3d* phase transitions, observed in ANBC and BABH, are reasonable if we assume that they are essentially the same phase in spite of the inverted phase sequence. The slope is about 0.5 J K^{-1} (mol of methylene)$^{-1}$ in both cases. The magnitude corresponds to the increase of the number of microscopic states by only a few per cent. This demonstrates a strong capability of chemical thermodynamics for a very complex system: The most macroscopic measurement offers the most microscopic information for a very complex system

Since the chain contribution is positive from the slope of this plot, there must be a negative contribution for the negative entropy of transition as a net for BABH. The other part than the alkyl chain is the hard core of the molecule. That is, the contribution of the core is negative in BABH. This also applies to ANBC because it is hard to imagine that a long chain such as $n = 12$ does not contribute any. The negative core contribution means that the cores are more ordered in the cubic phase than the SmC phase. Thus, it becomes clear that there is an entropic competition between the alkyl chain and molecular core in this SmC–cubic phase transition.

The inverted phase sequence between ANBC and BABH can be understood as shown in Fig. 8. The contribution of the core is negative and in the figure is assumed to be the same in ANBC and BABH. On the other hand, the contribution of the chain is positive and depends on its length. In ANBC having long chains, the net entropy of transition becomes positive and shows the SmC–cubic phase transition on heating. On the other hand, the entropy gain by the chain is insufficient to overcome the negative core contribution in BABH, resulting in the cubic–SmC phase transition on heating. In this way, we find the other role of the alkyl chain, entropy reservoir.

The above analysis predicts the inversion of the phase sequence even in BABH upon chain elongation. This is not realized in the normal pressure as seen in the phase diagram in Fig. 3. However, recently, Maeda and Yokoyama [43] reported that the SmC phase transforms to a cubic phase in BABH with longer chains with increasing temperature in accordance with the entropy analysis.

A similar inversion of the phase sequence takes place between the gyroid and *Im3m* phases in BABH(13) and BABH(16) as shown in Fig. 3 [13]. This inversion is also explained on the basis of the different degree of the order (entropy) of the alkyl chain appearing in the different slopes in Fig. 7 [24]: The alkyl chain is more disordered in the gyroid phase than in the *Im3m* phase.

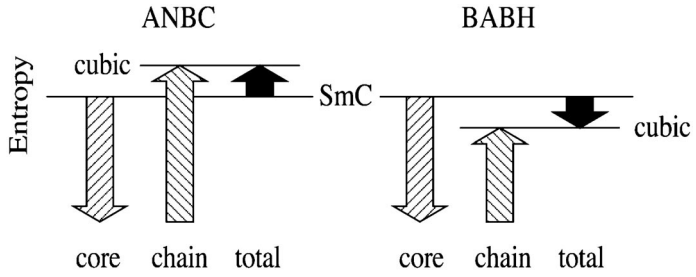

Fig. 8 "Alkyl-chains as entropy reservoir" mechanism for the inverted phase sequence between ANBC and BABH [24]. The shaded arrows orienting up and down indicate the opposite contribution to entropy from the chain and the core part, respectively, while the solid arrow corresponds to the net entropy resulting from their competing effect.

STRUCTURAL CHARACTERISTICS OF THE CUBIC LIQUID-CRYSTALLINE PHASE

Up to now, molecular details of mulicontinuous phases are not concerned. Here, we start the discussion on their structures. Figure 9 shows patterns of small-angle X-ray diffraction of BABH in isotropic liquid, *Im3m* and *Ia3d* cubic phases [13]. By indexing the diffractions, the cell dimensions are determined. Assuming the density to be ca. 1 g cm^{-3}, a unit cell of the cubic phases is considered to contain several hundreds to a few thousands molecules depending on the chain length (and temperature).

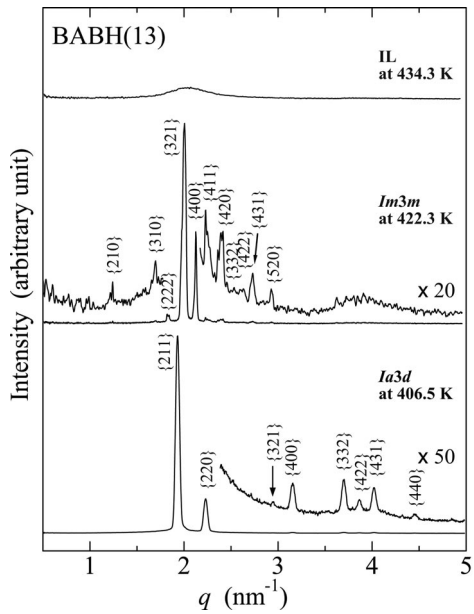

Fig. 9 Small-angle X-ray scattering patterns from the isotropic liquid (IL, top), and *Im3m* phase (middle) and *Ia3d* (bottom) phase of BABH(13) [13,48]. The broad halo peak (in the isotropic liquid) reflecting the density fluctuation with the wave vector that corresponds to the molecular length grows and condenses into some sharp peaks including {321} and {400} diffractions of the *Im3m* phase. At a lower temperature, the phase transition occurs to the *Ia3d* (gyroid) phase, whose {211} and {220} diffractions remain near the top of the halo peak in the isotropic liquid.

The comparison of the cell parameters of two cubic phases of the same compound would show a hint concerning the structure, because the local structure such as the curvature of the sheet-like aggregate is expected to remain the same for a given molecule even in different structures. The ratio of the cell parameters is 1.6 [12] for some members undergoing phase transitions between the two cubic phases. The most simple and well-known cubic structure having the space group *Im3m* is characterized by a TPMS called the P surface [15]. Gyroid and P surface is related by a mathematical transformation as described before. In this case, the cell parameter should have the ratio about 0.8. Since the ratio is definitely different from the observed one, it is concluded that the *Im3m* phase in ANBC and BABH is not simply related to the P surface. Hołyst and coworkers [20] predicted more complex structures with *Im3m* on the basis of a physical model of lyotropic systems. According to their prediction, there is a structure having the ratio about 1.5. In the spirit of the quasi-binary picture of thermotropics [39], it is thus natural to adopt this structure as the starting point. This structural model is characterized by two equivalent P-like surfaces located separately on both sides of the (mathematical) P surface. The same structural model was proposed by Kutsumizu [38] independently on the basis of totally different reasoning.

MOLECULAR AGGREGATION IN THE GYROID PHASE

Two complementary descriptions of the gyroid phase are given in Fig. 4. If the molecular cores are on the jungle gyms, the terminal methyl groups are around a (mathematical) gyroid surface. On the other hand, the cores form the gyroid if the methyl groups are on the jungle gyms. In this sense, knowing molecular packing is equivalent to locating the cores on the surface or on the jungle gym.

For systems having periodicity, diffraction is the most convenient and powerful tool as is widely used for crystal structure determination. However, there is a serious problem if we want to apply diffraction analysis to studying the structure of liquid crystals. The point is related to the Babinet principle. Diffraction experiments measure the intensity of the diffracted wave, which is only related to the absolute value of the structure factor. The structure factor is a Fourier transform of the distribution of scatterers such as electrons. Suppose hypothetical distribution patterns of the scatterer, A and B, which give the uniform, flat density upon summation. The structure factors F_A and F_B have the same magnitude with opposing signs except for a zero scattering vector ($\boldsymbol{q} = 0$). That is, the diffraction intensity is exactly the same for these two electron density distributions except for $\boldsymbol{q} = 0$.

Although the situation considered is the case even for normal crystals of small molecules, this does not become a serious issue because we know the electron has a large density peak on atoms. The correct density distribution can be chosen without any difficulty. However, the situation drastically changes if we consider liquid crystals. Since molecules are dynamically disordered, peaks cannot be assumed for individual atoms. Usually, the electron densities are approximated by a continuous (smooth) distribution without singular structures. In our case, the core has a higher electron density than the alkyl chain. There is another difficulty in the present case. The cubic phases generally appear in the concentration range slightly deviated from the equivolume concentration of the two components. Consequently, the volumes with high and low electron densities are nearly equal to each other. Because of these two difficulties, locating molecules within a unit cell is, in principle, impossible on the basis of the diffraction experiments on a single compound.

For the gyroid phase, the experimental patterns of the diffraction intensities of ANBC and BABH qualitatively coincide with the theoretical calculation for physical systems. The comparison is, therefore, the way we are able to adopt. There are many calculations of the diffraction intensities for structures related to gyroid. Among many calculations of the diffraction intensities, the work by Hołyst and a coworker [44–46] is the most systematic. They showed that the structure factors of a physical system are approximated by the product of the structure factor of the ideal, mathematical gyroid with zero thickness and a correcting factor for finite thickness. According to them, the ratio of the two strongest diffractions, {211} and {220}, decreases with increasing thickness.

Experimental ratio against the chain length is shown in Fig. 10 [47]. The two dotted levels are the calculated ratios for the volume fraction of the gyroid-forming part of 0.4 and 0.6 [44]. As the chain length certainly parallels the thickness of the volume fraction of the electron-deficient part, the decrease of the ratio clearly indicates that the chain decorates the gyroid. The terminal methyl groups are around the mathematical gyroid (with zero thickness). The cores are on the jungle gyms.

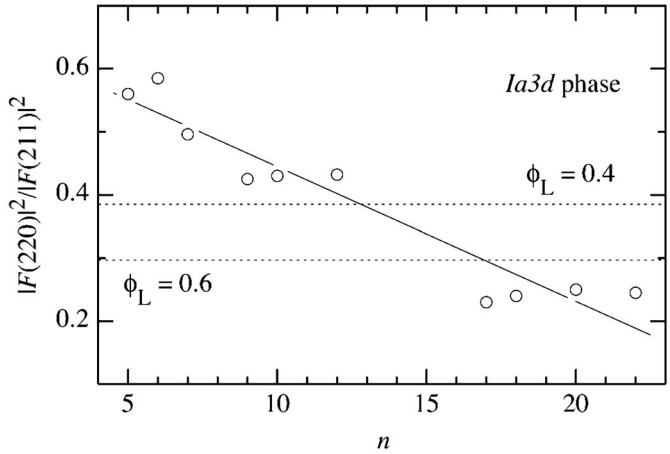

Fig. 10 Plots of the relative intensity of the {220} reflection with respect to the {211} reference peak as a function of *n* [47], which are compared with two values (dotted lines) calculated by Garstecki and Hołyst [44] for the volume fraction 0.4 and 0.6 of the gyroid-forming component. The solid line is a guide for eyes.

Figure 10 shows two additional features. The first point is that the region of the *Im3m* phase is around 0.5 in the volume fraction of the gyroid-forming part. In most theoretical works, the region containing equivolume for two components are of the lamellar phase characterized by flat surfaces. This suggests some connection between the Sm phase and the *Im3m* phase. The second feature is that the decrease seems to continue with an intermission by the region of the *Im3m* phase. This is rather surprising and in contradiction with simple theories. According to naïve understanding and most theories, the roles of two components are interchanged at the equivolume concentration. If this occurs, the ratio of diffractions should show an increase after passing through the region of the *Im3m* phase. In this sense, the present systems certainly have different properties from the lyotropic systems, which is well described by continuum theories. This behavior can be understood in the context of the Landau theory of the weak crystallization discussed in the next section [48].

LANDAU THEORY OF THE *Im3m* PHASE

The *Im3m* phase is located in-between the gyroid phases in both ANBC and BABH as seen in Fig. 3 [12,13]. There is no theory predicting the formation of an *Im3m* phase around this location. Assuming the PP model of the *Im3m* phase [20,35,38], two complementary structures can be constructed as in the case of the gyroid phase. Unfortunately, however, the distribution of the diffraction intensities is largely different from those calculated for both complementary structures. Consequently, the same strategy that is applied to the gyroid phase does not work for the *Im3m* phase.

Since the PP model is not a good model to interpret the diffraction intensities, before proceeding to the details of structure analysis, we need to construct a more reliable structural model. We here adopt the Landau theory of freezing. Landau theory is a phenomenological theory of phase transitions, and

based on the expansion of thermodynamic potential in terms of the relevant order parameter. In this sense, Landau theory is covered by thermodynamics in a broad context [28].

The application of Landau theory to freezing was done by Alexander and McTague [49]. They expanded the thermodynamic potential of isotropic liquid by density fluctuations as

$$f = \sum_{\mathbf{k}} \frac{1}{2} r_{\mathbf{k}} \left| n_{\mathbf{k}} \right|^2 - w \sum_{\mathbf{k}_1,\mathbf{k}_2,\mathbf{k}_3} n_{\mathbf{k}_1} n_{\mathbf{k}_2} n_{\mathbf{k}_3} \delta\left(\mathbf{k}_1 + \mathbf{k}_2 + \mathbf{k}_3\right) + u \sum_{\mathbf{k}_1,\mathbf{k}_2,\mathbf{k}_3,\mathbf{k}_4} n_{\mathbf{k}_1} n_{\mathbf{k}_2} n_{\mathbf{k}_3} n_{\mathbf{k}_4} \delta\left(\mathbf{k}_1 + \mathbf{k}_2 + \mathbf{k}_3 + \mathbf{k}_4\right) \quad (1)$$

where $n_{\mathbf{k}}$ is Fourier components of density fluctuation, and r, w, and u are expansion parameters. According to the symmetry of the isotropic liquid, there is the third-order term. This term is of the lowest order that can produce the periodic order in higher than one dimension. In this term, the δ-function exists. This means that the third-order term can survive only if the three wave vectors can form a triangle. That is, the ordered structure formed is characterized by the wave vectors that form the triangle.

In isotropic liquid, there is usually a strong density fluctuation with the wave vector corresponding to characteristic length. The fluctuation is observed as a broad halo in diffraction experiments. It is, therefore, reasonable to limit the summation only over wave vectors having this length. Indeed, by doing so, the superior stability of body-centered cubic structure was revealed by Alexander and McTague [49]. Since they considered simple liquid consisting of spherical particles, there is only one characteristic length scale. In the present case [48], on the other hand, the system consists of mesogenic molecules, which are roughly cylindrical. Cylinder has two characteristic lengths, height, and diameter. In the diffraction from the isotropic liquid shown in Fig. 9, a halo corresponding to the length of the molecule is clearly detected. Besides, the strong diffractions in the *Im3m* phase and the gyroid phase are limited in this region. It is thus natural to assume the importance of this wave vector.

We can find possible wave vectors that form equilateral triangles as {110}, {211}, {220}, {321}, {3,3,0}, {422}, {431}, {532}, ... in the order of the length of wave vectors. It is interesting to point out that the second and third vectors are the two strongest diffractions in the gyroid phase, on which more detailed discussion was performed within the Landau theory while taking the fluctuation effects into account [50]. On the other hand, the appearance of strong diffractions in the above series of wave vectors is only the case for the gyroid phase but not for structures characterized by other related TPMSs (P and D surfaces) [44]. This is possibly a cause for the superior stability of the gyroid phase [48].

The next wave vector {321} in the series capable of forming an equilateral triangle is one of two strongest diffractions of the *Im3m* phase. This strongly suggests the importance of this wave vector. Then, we need a further consideration on the other diffraction {400}, which is also very strong. The length of this wave vector (4) is very close to that of {321} ($\sqrt{3^2+2^2+1^2} = \sqrt{14} \approx 3.74$). This means that {400} is within a halo of the isotropic liquid reflecting strong density fluctuation. Besides, we can make mixed triangles like (3,2,1) + (–3,2,–1) + (0,–4,0) = (0,0,0). Therefore, wave vector {400} probably enhances the stability of the structure produced by the density fluctuation characterized by wave vector {321}.

Ignoring the wave vector dependence of the expansion coefficients, we can write out the thermodynamic potentials in terms of the magnitude of the density fluctuations characterized by wave vectors {321} and {400}. Assuming the temperature dependence only for r as usual, the freezing transition of the isotropic liquid to the cubic structure occurs at a transition temperature shown in Fig. 11 as a function of a, which is the ratio between density fluctuations characterized by wave vectors {321} and {400} defined as $a = n_{400}/n_{321}$. With increasing a, the transition temperature shows a maximum. As usual, the higher the transition temperature, the more stable the low-temperature phase. That is, the den-

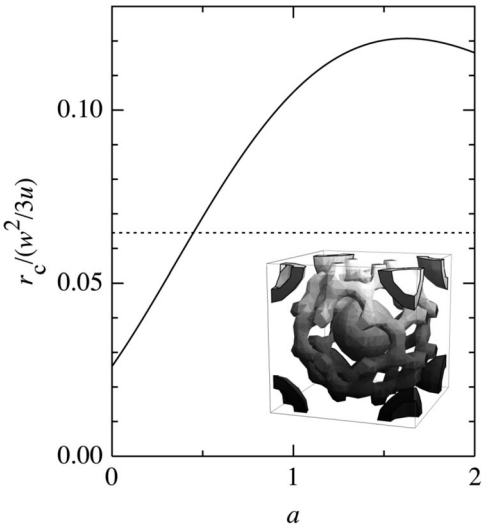

Fig. 11 Freezing transition temperature to the *Im3m* phase depending on the ratio $a = n_{400}/n_{321}$ of two density waves characterized by {321} and {400} assuming constant expansion parameters (w and u) [48]. The horizontal dotted line indicates the freezing transition temperature to the phase characterized by the single-density fluctuation {211}. The inset shows structural motifs within a unit cell formed by the density fluctuations characterized by {321} and {400}.

sity fluctuation characterized by {400} largely stabilizes the ordered structure [48]. It is emphasized that a must be positive for enhanced stability. This is an important point in the structure analysis.

The inset of Fig. 11 shows structural motifs found in the density distribution formed by density fluctuations characterized by wave vectors {321} and {400}. In reality, these are drawn as surfaces of constant density. There are two motives. One is a jungle gym extended over the whole system. The pipes of the jungle gym locate nearly on a minimal P surface. The other motifs are spherical shells at the body center and corners of the cell. The issue of the structure of the *Im3m* phase thus becomes which part of molecules forms these motifs.

MOLECULAR AGGREGATION IN THE *Im3m* PHASE

Finally, we reach the stage to discuss the molecular aggregation in the *Im3m* phase. In fact, there are reports of the structure of the *Im3m* phase [51,52], where the authors performed the small-angle X-ray diffraction experiments and reconstructed the structure by the conventional Fourier synthesis. Although the proposed structure is essentially compatible with the PP model [38,39], the analysis is incomplete especially for the selection of phase of diffracted waves, which is directly related to the location of the molecules.

We adopted the maximum entropy method (often abbreviated as MEM) [53,54] to reconstruct the electron density [55]. MEM is based on the information theory and gives the most probable and non-biased conclusion. In recent crystallography, the MEM is extensively used to improve the spatial resolution. There is, however, a problem in adopting the MEM. Usually, the MEM is used for an already known structure. On the other hand, in the present case, we have no correct solution. We therefore need to modify the MEM algorithm to take the information of phase (sign in reality because of the presence of the inversion in *Im3m* symmetry) of diffractions only for {321} and {400}. All four combinations are assumed in calculations. For other diffractions, only the intensity was considered.

Starting from the flat density of electron density, MEM iterations converged successfully in all combinations of phases for {321} and {400}. Since structure factors are Fourier components of density wave weighted by electron density, they are approximates of the density fluctuation considered in the Landau theory [48]. Therefore, the theory strongly suggests that the ratio of these two diffractions is positive. This is equivalent to the fact that the signs are the same for them. On the other hand, the molecular structure of BABH shows that the volume of the core part is obviously smaller than that of the chain. This means that the volume fraction of the higher density than the average should be less than half. These requirements are fulfilled only when the signs are chosen as (–, –) for {321} and {400}.

In this way, we reach the structure of the *Im3m* phase shown in Fig. 12. The structural motifs are formed by molecular cores having the higher electron density. There are two types. One motif is a jungle gym extended over the whole system. The junction is three-fold as in the interwoven jungle gyms of the gyroid phase, which also consist of molecular cores. The other motif is a spherical shell. The shell can be regarded as a sheet-like aggregate common to the Sm phase. The *Im3m* phase, thus, has similarities to both the gyroid and Sm phases, consistent with its location in the phase diagram [12,13].

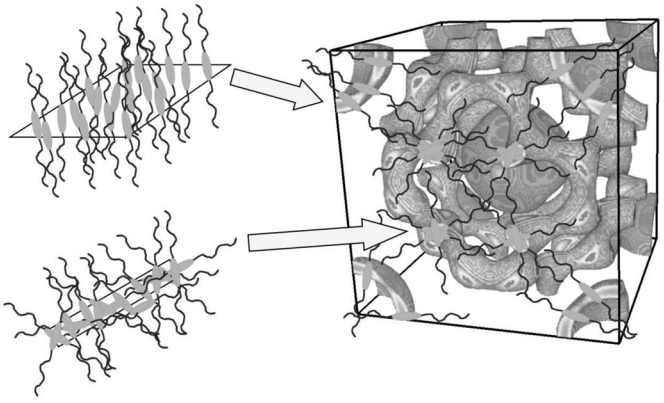

Fig. 12 High electron density region in a unit cell of the *Im3m* phase of BABH(15) reconstructed by the MEM analysis adopting the phase combination (–,–) for {321} and {400} diffractions [55].

CONCLUSIONS

Extensive application of chemical thermodynamics to exotic aggregation formed in thermotropic liquid crystal is briefly described. The multicontinuous structure suppresses the fluctuation due to three-dimensional connectivity as evidenced by the precise heat capacity calorimetry. In the formation of a variety of liquid-crystalline phases, the alkyl chains attached to the molecular rigid core serves as a self-solvent as demonstrated through the comparison of phase diagrams. This is the experimental basis for the "quasi-binary picture of thermotropics," which puts a possible framework for the unified understanding of thermotropic and lyotropic liquid crystals. The analysis of the chain-length dependence of entropy of transition (ΔS analysis) leads us to find a new role of alkyl chains as "entropy reservoir," which induces the inverted phase sequence in the SmC–*Ia3d* and *Ia3d*–*Im3m* phase transitions, arising from the entropic competition between the alkyl chain and molecular core. Thermodynamic theory of phase transition puts a basis for understanding the superior stability of the gyroid phase and the formation mechanism of the *Im3m* phase, and for revealing the molecular aggregation mode in the *Im3m* phase. In conclusion, thermodynamics is a powerful and indispensable framework for the science of complex systems.

ACKNOWLEDGMENTS

The contents of the review represents selections from research activities during more than 10 years with many collaborators, to all of whom thanks are due. Especially, the author thanks Prof. M. Sorai who introduced him to this fascinating field and Prof. S. Kutsumizu for a long collaboration. Besides, fruitful discussions were invaluable with Profs. T. Dotera and T. Ohta, and with Dr. R. Pełka. The works were supported in part by a Grant-in-Aid for Scientific Research (A) (No. 11304050) from the Ministry of Education, Culture, Sports, Science and Technology, Japan (MEXT), a Grant-in-Aid for Scientific Research (B) (No. 15350110) from the Japan Society for the Promotion of Science, and a Grant-in-Aid for Scientific Research on Priority Area "Non-Equilibrium Soft Matter" (No. 463/19031002) from MEXT.

REFERENCES

1. P. G. de Gennes, J. Prost. *The Physics of Liquid Crystals*, Clarendon Press, Oxford (1993).
2. J. A. Pople, F. E. Karasz. *J. Phys. Chem. Solids* **18**, 28 (1961).
3. S. Chandrasekhar, R. Shashidhar, N. Tara. *Mol. Cryst. Liq. Cryst*. **10**, 337 (1970).
4. P. Bolhuis, D. Frenkel. *J. Chem. Phys*. **106**, 666 (1997).
5. L. Onsager. *Ann. N.Y. Acad. Sci*. **51**, 627 (1949).
6. G. Gompper, M. Schick. *Self-Assembling Amphiphilic Systems, Phase Transitions and Critical Phenomena*, Vol. 16, C. Domb, J. L. Lebowitz (Eds.), Academic Press, San Diego (1994).
7. A. M. F. Neto, S. R. A. Salinas. *The Physics of Lyotropic Liquid Crystals*, Oxford University Press, Oxford (2005).
8. G. W. Gray, B. Jones, F. Marson. *J. Chem. Soc*. 393 (1957).
9. D. Demus, A. Gloza, H. Hartung, A. Hauser, I. Rapthel, A. Wiegeleben. *Cryst. Res. Technol*. **16**, 1445 (1981).
10. S. Kutsumizu, R. Kato, M. Yamada, S. Yano. *J. Phys. Chem. B* **101**, 10666 (1997).
11. K. Saito, T. Shinhara, M. Sorai. *Liq. Cryst*. **27**, 1555 (2000).
12. S. Kutsumizu, K. Morita, T. Ichikawa, S. Yano, S. Nojima, T. Yamaguchi. *Liq. Cryst*. **29**, 1447 (2002).
13. S. Kutsumizu, H. Mori, M. Fukatami, S. Naito, K. Sakajiri, K. Saito. *Chem. Mater*. **20**, 2675 (2008).
14. S. Kutsumizu, T. Ichikawa, S. Nojima, S. Yano. *Chem. Commun*. 1181 (1999).
15. S. Hyde, S. Andersson, K. Larsson, Z. Blum, T. Landh, S. Lidin, B. W. Ninham. *The Language of Shape*, Elsevier, Amsterdam (1997).
16. I. W. Hamley. *The Physics of Block Copolymers*, Oxford University Press, Oxford (1998).
17. L. Leibler. *Macromolecules* **13**, 1602 (1980).
18. T. Ohta, K. Kawasaki. *Macromolecules* **19**, 2621 (1986).
19. M. W. Matsen, F. S. Bates. *Macromolecules* **29**, 1091 (1996).
20. W. T. Góźd , R. Hołyst. *Phys. Rev. E* **54**, 5012 (1996).
21. A. Sato, Y. Yamamura, K. Saito, M. Sorai. *Liq. Cryst*. **26**, 1185 (1999).
22. N. Morimoto, K. Saito, Y. Morita, K. Nakasuji, M. Sorai. *Liq. Cryst*. **26**, 219 (1999).
23. A. Sato, Y. Yamamura, K. Saito, M. Sorai. *Liq. Cryst*. **26**, 1185 (1999).
24. K. Saito, T. Shinhara, T. Nakamoto, S. Kutsumizu, S. Yano, M. Sorai. *Phys. Rev. E* **65**, 031719 (2002).
25. M. Sorai, K. Saito, T. Nakamoto, M. Ikeda, Y. G. Galyametdinov, I. Galyametdinova, R. Eidenschink, W. Haase. *Liq. Cryst*. **30**, 861 (2003).
26. M. Nishizawa, K. Saito, M. Sorai. *J. Phys. Chem. B* **105**, 2987 (2001).
27. K. Saito, N. Kitamura, M. Sorai. *J. Phys. Chem. B* **107**, 7854 (2003).

28. L. D. Landau, E. M. Lifshitz. *Statistical Physics, Part 1*, 3rd ed., Pergamon Press, New York (1980).
29. T. Yamaguchi, M. Yamada, S. Kutsumizu, S. Yano. *Chem. Phys. Lett*. **240**, 105 (1995).
30. S. Kutsumizu, T. Yamaguchi, R. Kato, S. Yano. *Liq. Cryst*. **26**, 567 (1999).
31. J. C. Eriksson, S. Ljunggren. *J. Colloid Interface Sci*. **167**, 227 (1994).
32. S. Kutsumizu. *Curr. Opin. Solid State Mater. Sci*. **6**, 537 (2002).
33. R. Tamate, K. Yamada, J. Viñals, T. Ohta. *J. Phys. Soc. Jpn*. **77**, 034802 (2008).
34. M. Sorai, K. Tsuji, H. Suga, S. Seki. *Mol. Cryst. Liq. Cryst*. **80**, 33 (1980).
35. M. Sorai, K. Saito. *Chem. Rec*. **3**, 29 (2003).
36. G. W. Smith. *Mol. Cryst. Liq. Cryst*. **49**, 207 (1979).
37. K. Saito, A. Sato, M. Sorai. *Liq. Cryst*. **25**, 525 (1998).
38. S. Kutsumizu, K. Morita, S. Yano, S. Nojima. *Liq. Cryst*. **29**, 1459 (2002).
39. K. Saito, M. Sorai. *Chem. Phys. Lett*. **366**, 56 (2002).
40. M. Yoneya, K. Araya, E, Nishikawa, H. Yokoyama. *J. Phys. Chem. B* **108**, 8099 (2004).
41. S. Kutsumizu, M. Yamada, S. Yano. *Liq. Cryst*. **16**, 1109 (1994).
42. K. Saito, M. Ikeda, M. Sorai. *J. Therm. Anal. Calor*. **70**, 345 (2002).
43. Y. Maeda, H. Yokoyama. *Thermochim. Acta* **441**, 156 (2006).
44. P. Garstecki, R. Hołyst. *J. Chem. Phys*. **113**, 3772 (2000).
45. P. Garstecki, R. Hołyst. *Langmuir* **18**, 2519 (2002).
46. P. Garstecki, R. Hołyst. *Langmuir* **18**, 2529 (2002).
47. S. Kutsumizu, H. Mori, M. Fukatami, K. Saito. *J. Appl. Crystallogr*. **40**, s279 (2007).
48. K. Saito, Y. Yamamura, S. Kutsumizu. *J. Phys. Soc. Jpn*. **77**, 093601 (2008).
49. S. Alexander, J. McTague. *Phys. Rev. Lett*. **41**, 702 (1978).
50. V. E. Podneks, I. W. Hamley. *JETP Lett*. **64**, 617 (1996).
51. X. Zeng, G. Ungar, M. Impéror-Clerc. *Nat. Mater*. **4**, 562 (2005).
52. X. Zeng, L. Cseh, G. H. Mehl, G. Ungar. *J. Mater. Chem*. **18**, 2953 (2008).
53. D. M. Collins. *Nature* **298**, 49 (1982).
54. M. Sakata, M. Sato. *Acta Crystallogr., Sect. A* **46**, 263 (1990).
55. K. Ozawa, Y. Yamamura, Y. Yasuzuka, H. Mori, S. Kutsumizu, K. Saito. *J. Phys. Chem. B* **112**, 12179 (2008).